Optimal FX Market Making under Inventory Risk and Adverse Selection Constraints

Sid Ghoshal
University of Oxford
siddartha.ghoshal@eng.ox.ac.uk

Stephen Roberts
University of Oxford
sjrob@robots.ox.ac.uk

Abstract

Market makers are faced with the complex optimisation problem of maximising their profit while minimising their inventory risk. This dual mandate exerts inherently opposing forces: the simplest way to avoid inventory is to maintain wide bid-offer spreads, yet doing so will prevent deal flow and therefore neuter profitability. Conversely, showing competitive two-way prices will ensure heavier volumes on both sides of the order book and therefore lock-in gains from clients crossing the bid-offer spread, but opens the hazard of building up sizeable inventory risk if trade flow is temporally asymmetric. A further concern for dealers is the threat of adverse selection by market professionals exploiting an information advantage. Existing work in finance and stochastic control provides a robust framework for dynamically balancing inventory, but does little to address adverse selection in over-the-counter markets where prices can be individually tuned for each counterparty. In this paper, we consider a data-driven adjustment to the state-of-the-art model based on the entropy of a high-dimensional, probabilistic representation of each connection's behaviour. Bayesian community detection techniques are applied to an adjacency matrix of broker distributions, to reduce dimensionality and guarantee the scalability of our approach. Our entropy metrics provide a basis for measuring adverse selection and feed directly into the Hamilton-Jacobi-Bellman framework for deriving inventory-optimal bid and offer prices.

I. Introduction

Market makers are tasked with providing liquidity by quoting two prices, their bid and offer, reflecting where they are willing to buy and sell a fixed quantity of an asset. The gap between these prices, locked in as profit for every contemporaneous buy and sell order of identical size, exists to compensate dealers for their two main sources of risk: *inventory risk* and *adverse selection risk*.

Inventory risk stems from variations in the value of the asset held, and adverse selection refers to instances where knowledgeable counterparties take advantage of information asymmetry to build an (eventually) lucrative position, to the detriment of the market maker. Stochastic control models pioneered by Ho and Stoll [1] and further developed by Avellaneda and Stoikov [2] provide a robust framework for dynamically adjusting bid and offer prices to manage asset-specific inventory risk. Adverse selection, however, is a client-specific risk that does not readily fit with the Hamilton-Jacobi-Bellman approach.

Over-the-counter (OTC) FX markets differ

materially from the on-exchange equity markets studied in the stochastic control literature. Liquidity providers in an OTC setting can show different quotes to each connection, relying on their knowledge of the counterparty's price elasticity to optimise bid and offer levels. This paper explores Bayesian representations of client behaviour, in an effort to quantify adverse selection and thereby adjust bid and offer prices punitively for counterparties whose trades are deemed opportunistic.

We produce multivariate Automatic Relevance Determination (ARD) Gaussian Process representations of each connection, pairing trade activity with market data metrics such as time of day, volatility, short-term returns and bid-offer spread. We show evidence of predictability in client responses to market conditions, and construct a matrix of Bhattacharyya distances to measure the similarity of connections to each other. In the interest of scalability, we reduce the problem's dimensionality by clustering counterparties with a community detection technique built on Bayesian non-Negative Matrix Factorisation. Finally, we demonstrate how the notion of counterparty entropy can be integrated into an augmented Hamilton-Jacobi-Bellman (HJB) framework to control for both inventory risk and adverse selection risk simultaneously.

II. Stochastic Control Modelling

We begin with a summary of the state-of-the-art model for managing inventory risk, defining the value function of the market maker before drawing on results in control theory literature to solve for utility maximisation.

I. The Market Maker Value Function

We define the market maker's bid-mid and mid-offer price gaps as

$$\delta^b = s - p^b \tag{1}$$

$$\delta^a = p^a - s \tag{2}$$

where s is an exogeneously-defined mid-market price, and p^b and p^a are the market maker's bid and ask prices. We follow Avellaneda and Stoikov in the assumption that a market maker's buy and sell limit orders are filled at a Poisson rate $\lambda^b(\delta^b)$ and $\lambda^a(\delta^a)$, decreasing functions of their respective arguments.

Using the utility framework of Ho and Stoll, we parametrise the following value function for the market maker:

$$v(x, s, q, t) = E_t[-\exp(-\gamma(x + qS_T))] \tag{3}$$

where x is the market maker's wealth, s is the mid price, q is the current inventory (which can be negative, when shorting), γ is a discount factor and t is time. We can then define the market maker's *reservation* or *indifference* bid and ask prices r^b and r^a using the relations

$$v(x - r^b(s, q, t), s, q + 1, t) = v(x, s, q, t) \tag{4}$$

$$v(x + r^a(s, q, t), s, q - 1, t) = v(x, s, q, t) \tag{5}$$

The average of r^b and r^a in Equations (4) and (5) provides the market maker's indifference price, and constitutes a divergence from the fair mid that decreases monotonically with inventory level.

II. The Hamilton-Jacobi-Bellman Equation

The dealer's objective is given by the value function:

$$u(x, s, q, t) = \max_{\delta^b, \delta^a} E_t[-\exp(-\gamma(x + qS_T))] \tag{6}$$

where δ^b and δ^a can be thought of as feedback controls. A key finding in the works of Ho and Stoll was the application of the dynamic programming principle to show that the function u solves the following Hamilton-Jacobi-Bellman

equation:

$$\begin{cases} u_t + \frac{1}{2}\sigma^2 u_{ss} + \max_{\delta^b} \lambda^b(\delta^b)\big[u(s, x-s+\delta^b, \\ q+1, t) - u(s,x,q,t)\big] + \max_{\delta^a} \lambda^a(\delta^a)\big[u(s, \\ x+s+\delta^a, q-1, t) - u(s,x,q,t)\big] = 0 \\ u(s,x,q,T) = -\exp(-\gamma(x+qs)) \end{cases} \tag{7}$$

Avellaneda and Stoikov's choice of an exponential utility allows a simplification of the problem. They postulate that there exists a function θ such that

$$u(x,s,q,t) = -\exp(-\gamma x)\exp(-\gamma\theta(s,q,t)) \tag{8}$$

Direct substitution of Equation (8) into Equation (7) yields the following system for θ:

$$\begin{cases} \theta_t + \frac{1}{2}\sigma^2\theta_{ss} - \frac{1}{2}\sigma^2\gamma\theta_s^2 + \max_{\delta^b}\left[\frac{\lambda^b(\delta^b)}{\gamma} \right. \\ \left.\big[1-\exp(\gamma(s-\delta^b-r^b))\big]\right] + \max_{\delta^a}\left[\frac{\lambda^a(\delta^a)}{\gamma} \right. \\ \left.\big[1-\exp(-\gamma(s+\delta^a-r^a))\big]\right] = 0 \\ \theta(s,q,T) = qs \end{cases} \tag{9}$$

Furthermore, applying Equation (8) to the reservation bid and ask prices given by Equations (4) and (5) yields the relations

$$\delta^b_{HJB} = s - r^b(s,q,t) + \frac{1}{\gamma}\log\left(1-\gamma\frac{\lambda^b(\delta^b)}{(\partial\lambda^b/\partial\delta)(\delta^b)}\right) \tag{10}$$

and

$$\delta^a_{HJB} = r^a(s,q,t) - s + \frac{1}{\gamma}\log\left(1-\gamma\frac{\lambda^a(\delta^a)}{(\partial\lambda^a/\partial\delta)(\delta^a)}\right) \tag{11}$$

The HJB solution to inventory risk management can be viewed as a two-step process: first solve for $r^b(s,q,t)$ and $r^a(s,q,t)$ in the PDE given by Equation (9), then solve Equations (10) and (11) to obtain the optimal distance $\delta^b_{HJB}(s,q,t)$ and $\delta^a_{HJB}(s,q,t)$ between the mid price and the optimal bid and ask quotes.

III. Data

In this section we describe both the market maker dataset provided by BNP Paribas, and the market metrics derived from EURUSD tick data for the same time period.

I. The BNP Paribas FX Dataset

The BNP Paribas dataset includes a large set of FX trades executed by their market makers in 2013. The complete dataset counts 916,683 trades split across 12 currencies, with EURUSD by far the most actively traded pair. For each trade, the raw dataset provides a timestamp, the currency pair, deal size, whether it was a buy or a sell, as well as both client ID and broker ID numbers. In the analysis that follows, we restrict our attention to EURUSD trades taking place in January 2013 - this dataset's dealcount is 35,001, large enough to remain representative. Figure 1 overleaf provides the full currency breakdown for the January 2013 subset.

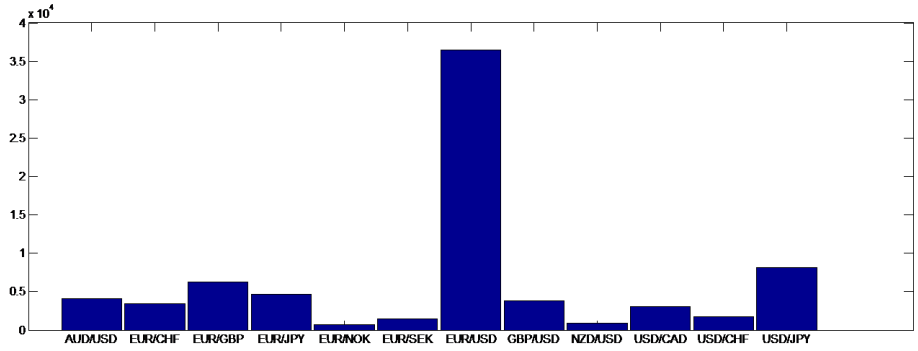

Figure 1: Histogram of tradecount by currency in the BNP Paribas dataset for January 2013, N=74958. Note that 46.7% of trade orders are in EURUSD.

II. EURUSD Tick Data

The EURUSD tick dataset provided by Pepperstone Group provides high-frequency bid and offer prices for 2013. The tick data for January 2013 alone contains 10,133,449 entries and allows us to produce 7 market-derived features to better understand client sensitivity.

• The time of day feature returns the decimal part of each timestamp, to track intraday seasonality effects.

• Two volatility metrics were constructed to account for tradeflow reacting to volatility ('lagging volatility') and tradeflow anticipating volatility ('leading volatility'). In particular, a significant bias in the latter may indicate an information advantage as the client's activity foreshadows rapid change in market conditions.

$$\text{1-minute Lagging Volatility(t)} = \sqrt{\frac{1}{N_t}\sum_{t\in[t,t+1m]}\Big(\text{EURUSD(mid)}_t - \mu_{t\in[t,t+1m]}\Big)^2}$$

$$\text{1-minute Leading Volatility(t)} = \sqrt{\frac{1}{N_t}\sum_{t\in[t-1m,t]}\Big(\text{EURUSD(mid)}_t - \mu_{t\in[t-1m,t]}\Big)^2} \quad (12)$$

(13)

• Three return metrics were devised to search for systematic bias in a client's returns at various timescales. A systematic positive bias in an individual connection's trade returns would provide strong evidence of adverse selection.

$$\text{1-minute Return(t)} = \frac{\text{EURUSD(mid)}_{t+1m} - \text{EURUSD(mid)}_t}{\text{EURUSD(mid)}_t} \quad (14)$$

$$\text{1-hour Return(t)} = \frac{\text{EURUSD(mid)}_{t+1h} - \text{EURUSD(mid)}_t}{\text{EURUSD(mid)}_t} \quad (15)$$

$$\text{1-day Return(t)} = \frac{\text{EURUSD(mid)}_{t+1d} - \text{EURUSD(mid)}_t}{\text{EURUSD(mid)}_t} \quad (16)$$

• Finally, we include bid-offer spreads as a proxy for market-wide volumes.

$$\text{Bid-Offer Spread(t)} = \text{EURUSD(offer)}_t - \text{EURUSD(bid)}_t \quad (17)$$

IV. ARD Gaussian Processes

We briefly recall the fundamentals of Gaussian Process modelling before describing ARD kernels and the associated relevance metrics. For

a comprehensive treatment of Gaussian Processes, please refer to [4].

A Gaussian Process is a collection of random variables, any finite subset of which has a joint Gaussian distribution. Gaussian Processes are fully parametrised by a mean function and covariance function, or kernel. Given a real process $f(\mathbf{x})$, we write the Gaussian Process as:

$$f(\mathbf{x}) \sim \mathcal{GP}(m(\mathbf{x}), k(\mathbf{x}, \mathbf{x}')) \tag{18}$$

where functions $m(\mathbf{x})$ and $k(\mathbf{x},\mathbf{x}')$ are respectively the mean and covariance functions:

$$m(\mathbf{x}) = \mathbb{E}[f(\mathbf{x})] \tag{19}$$

$$k(\mathbf{x}, \mathbf{x}') = \mathbb{E}[(f(\mathbf{x}) - m(\mathbf{x})) \times (f(\mathbf{x}') - m(\mathbf{x}'))] \tag{20}$$

Inputs are commonly centred during pre-processing, meaning the GP is fully specified by the form of its kernel. A common choice in finance is the Matérn 3/2 kernel, a once-differentiable function exhibiting the low smoothness typical of return series.

$$k(\mathbf{x}, \mathbf{x}') = \sigma_f^2 \Big(1 + \frac{\sqrt{3}|\mathbf{x} - \mathbf{x}'|}{l}\Big) \times \exp\Big(-\frac{\sqrt{3}|\mathbf{x} - \mathbf{x}'|}{l}\Big) \tag{21}$$

The covariance function above employs an isotropic Manhattan norm as the similarity measure between two vectors in input space. This assumes that a single, global characteristic length scale l can appropriately evaluate proximity in all input dimensions. Even with all inputs normalised to the same scale during pre-processing, it is likely that they will contain varying levels of information on the output variable, motivating the use of input-specific characteristic length scales.

In ARD kernels, the scalar input length scale l of Equation (21) is replaced with a vector input length scale with a different l_i for each input dimension i, allowing for different distance measures. These hyperparameters will adapt to any given dataset: inputs with large length scales cause only marginal variations in the covariance function, whereas inputs with small length scales effectively magnify those variations. We can therefore define the relevance score of each feature to be the reciprocal of its input length scale, and rank the salience of inputs by descending relevance.

$$\text{Relevance Score}_i = l_i^{-1} \tag{22}$$

A limitation of the methodology is that the relevance scores only provide a relative ranking between the features of a model. Two equally meaningless inputs will have relevance scores of similar magnitude, as would two equally meaningful features. On their own, these scores provide little basis for performing dimensionality reduction. To overcome this, we include in each regression a baseline feature composed of standard Gaussian noise. Any meaningful input should have a relevance score that is at least two orders of magnitude greater than noise, so by computing the Relevance Ratio we can determine which features are objectively informative.

$$\text{Relevance Ratio}_i = \frac{\text{Relevance Score}_i}{\text{Relevance Score}_{noise}} \tag{23}$$

V. Application

In this section, we detail the results of our analysis. After preliminary client data exploration using kernel density estimators (KDEs), we determine significant correlations within the dataset and evaluate the ARD framework's ability to identify salience. With Gaussian Processes constructed for each connection, we define the Bhattacharyya distance between GPs and derive a similarity matrix on which to apply community detection techniques. Finally, we measure the entropy of each counterparty's dynamics and relate our findings to the HJB solution of Avellaneda and Stoikov.

I. Kernel Density Estimation

Univariate KDEs offer a first glimpse into aggregate client behaviour, by viewing tradeflow as a point process and assigning a Gaussian density to each datum. The resulting distribution provides a probabilistic interpretation of client activity, and yields intuitive findings concerning intraday seasonality and short-term return bias.

• Aggregate client activity peaks twice in the day, at 10:00 GMT and 15:00 GMT, reflecting high points in tradeflow for London and New York respectively. These spikes appear in Figure 2.

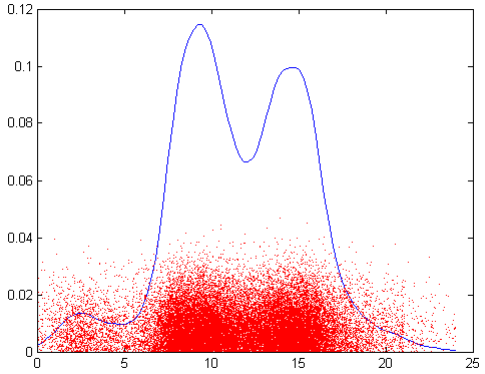

Figure 2: Kernel density estimator of January 2013 trades in EURUSD as a function of time of day, with scatter of individual trades, n=35001. The x-axis follows Greenwich Mean Time. For graphical clarity, each datapoint was jittered vertically with Gaussian noise.

• Client 1-min returns tend to be slightly negative, reflecting that price takers must pay half the spread to transact. Their trades execute at a small disadvantage to mid-market, and are therefore biased to remain that way in the very short term (Figure 3).

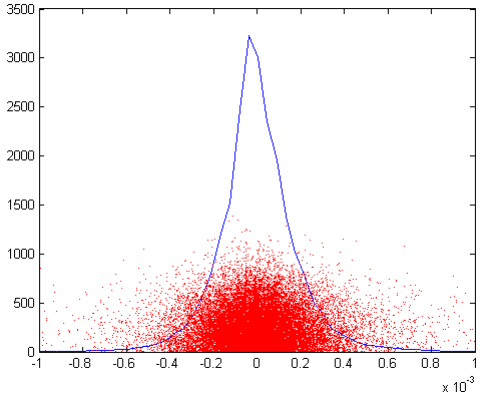

Figure 3: Kernel density estimator of January 2013 trades in EURUSD as a function of 1-minute returns, with scatter of individual trades, n=35001.

II. Correlation Analysis

A significant drawback of using kernel density estimation lies in its application of equal Gaussian densities for each trade, regardless of size. In reality, meaningful learning of client behaviour would require forecasting the circumstances in which their largest orders are placed. We conduct two separate correlation analyses, to account for the fact that certain features are sensitive to the polarity of traded volumes (that is, whether the order is a buy or a sell).

• Correlation between each market return metric and signed deal size. The results are provided in Table 1.

• Correlation between volatility, time of day, bid-offer spread and absolute deal size. The results are provided in Table 2.

We briefly outline a methodology for determining whether an observed sample correlation is significant. Given two independent random variables x_i and y of length N with sample correlation r, the statistic

$$t = \frac{r \times \sqrt{N-2}}{\sqrt{1-r^2}} \tag{24}$$

is t-distributed with N-2 degrees of freedom.

Table 1: *Correlation between Return Metrics and Signed Deal Size, N=35001.*

	Correlation		p-value	
Feature	Pearson	Spearman	Pearson	Spearman
1-min Return	$\mathbf{-0.0379}$	$\mathbf{-0.0405}$	$\mathbf{< 0.0001}$	$\mathbf{< 0.0001}$
1-hour Return	-0.0061	-0.0178	0.2516	0.0009
1-day Return	$+0.0032$	-0.0024	0.5494	0.6589

Table 2: *Correlation between Time of Day, Volatility, Bid-Offer Spread and Absolute Deal Size, N=35001.*

	Correlation		p-value	
Feature	Pearson	Spearman	Pearson	Spearman
Time of Day	$\mathbf{+0.0366}$	$\mathbf{+0.0134}$	$\mathbf{< 0.0001}$	$\mathbf{< 0.0001}$
1-min Lagging Volatility	$\mathbf{+0.0345}$	$\mathbf{+0.0801}$	$\mathbf{< 0.0001}$	$\mathbf{< 0.0001}$
1-min Leading Volatility	$\mathbf{+0.0478}$	$\mathbf{+0.0570}$	$\mathbf{< 0.0001}$	$\mathbf{< 0.0001}$
Bid-Offer Spread	-0.0047	$+0.0247$	0.3835	< 0.0001

Table 3: *Relevance across all polarity-sensitive features measured on the January 2013 dataset, N=35001.*

	Mean Relevance		Spearman	
Feature	Score	Ratio	Correlation	p-value
1-min Return	0.2	4.1	-0.0405	< 0.0001
1-hour Return	0.2	6.4	-0.0178	0.0009
1-day Return	0.2	4.5	-0.0024	0.6589

Table 4: *Relevance across all polarity-insensitive features measured on the January 2013 dataset, N=35001.*

	Mean Relevance		Spearman	
Feature	Score	Ratio	Correlation	p-value
Time of Day	5.8	11	$+0.0134$	< 0.0001
1-min Lagging Volatility	$\mathbf{1.2 \times 10^6}$	$\mathbf{2.3 \times 10^6}$	$\mathbf{+0.0801}$	$\mathbf{< 0.0001}$
1-min Leading Volatility	$\mathbf{7.4 \times 10^6}$	$\mathbf{1.3 \times 10^7}$	$\mathbf{+0.0570}$	$\mathbf{< 0.0001}$
Bid-Offer Spread	0.56	1.0	$+0.0247$	< 0.0001

Values for the *(r,N)* pair that land outside the 95% confidence interval of the t-distribution violate the null hypothesis of independence, providing a methodology known as Student's t-testing for identifying significant correlations in a dataset. P-values are derived from t-distribution tables and measure the probability that an uncorrelated data sample will yield a t-statistic as or more extreme than the value of t obtained from Equation (24). Common significance thresholds are p-values of 0.05 or 0.01.

Applying t-tests to our dataset, it quickly emerges that client activity is hugely sensitive to market movements, signalled by numerous p-values under 0.01 by several orders of magnitude in Tables 1 and 2.

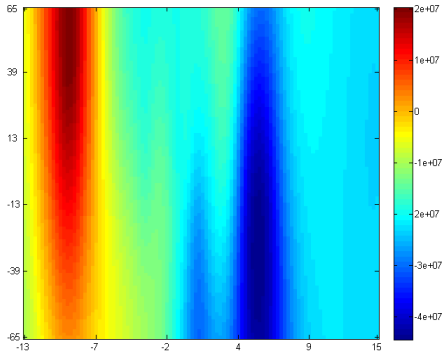

Figure 4: Signed Deal Volume for broker connection #1 as a function of 1-minute Returns (x-axis, in basis points) and 1-hour Returns (y-axis, in basis points), for connection #1. Large buy orders correlate with negative 1-min returns (peak red area corresponding to -0.09% return on the x-axis) and large sell orders correlate with positive 1-min returns (peak blue area corresponding to +0.05% on the x-axis). This matches the earlier finding of a strong negative correlation between signed deal size and 1-minute returns.

III. ARD-GP Representation of Counterparty Behaviour

The discovery of multiple significant correlations in our dataset motivates the search for a robust, multivariate probabilistic technique for modelling each connection's dynamics. ARD Gaussian Processes learn the respective relevances of each feature, and should therefore rank highest those features whose correlation is most significant.

We produce an ARD Gaussian Process for each individual connection, and provide in Tables 3 and 4 the mean Relevance Score and Relevance Ratio for each feature, alongside its Spearman correlation and p-value. Separate tables were necessary to reflect that certain features were regressed on, and correlate with, signed deal size whereas others were measured against absolute deal size.

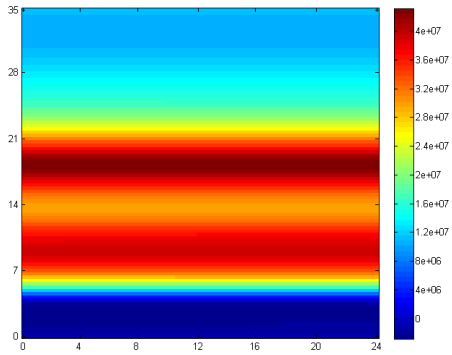

Figure 5: Absolute Deal Volume for broker connection #1 as a function of Time of Day (x-axis, in hours) and 1-minute Leading Volatility (y-axis, in percentage points). In the case of this connection, time of day was insignificant (correlation of +0.0128 with a p-value of 0.4137), with leading volatility dominating the forecast distribution (correlation of +0.0435 with a p-value of 0.0054, below the significance level of 0.01).

The ARD ranking tallies broadly with the results from the earlier correlation analysis on absolute deal sizes, but diverges materially from our expectations for the 1-min, 1-hour

Table 5: *Bayesian NMF clustering on the January 2013 dataset across 25 broker connections.*

Bayesian NMF Cluster	Nodes Assigned
Cluster 1 with membership score > 0.8	2, 3, 6, 7, 8, 15, 17, 19, 24
Cluster 2 with membership score > 0.8	1, 9, 10, 13, 14, 16, 18, 20, 21, 22, 23, 25
Overlap between Clusters	4, 5, 11, 12

and 1-day feature set. It nevertheless allows us to produce meaningful bivariate visualisations of client sensitivity to its dominant features. As an example of the framework's ability to represent behaviour, we provide heatmaps of broker connection #1's response to its most salient features in Figures 4 and 5.

IV. Community Detection

Having constructed Gaussian Processes for each connection, we wish to measure the similarity between behaviours in order to cluster counterparties and apply different adjustments to the HJB bid-offer price based on the cluster's entropy. In light of the extreme relevance scores found in the GPs regressing absolute volumes on time of day, volatility and bid-offer spread, we have adopted those features as our basis for community detection.

IV.1 Bhattacharyya Distance

Detection of clusters requires the creation of a matrix of distances that capture the pairwise overlap between any two connections [5]. GPs by definition have a probabilistic interpretation, as a draw from a probability distribution over functions. Amidst the wide range of available symmetric distance measures, we choose the Bhattacharyya distance as our measure of similarity between two probability distributions f and g, defined as

$$D_B(f(\mathbf{x}), g(\mathbf{x})) = -\log(BC(f(\mathbf{x}), g(\mathbf{x}))) \quad (25)$$

where $BC(f(\mathbf{x}),g(\mathbf{x}))$ is the Bhattacharyya Coefficient given by

$$BC(f(\mathbf{x}), g(\mathbf{x})) = \int \sqrt{f(\mathbf{x})g(\mathbf{x})}d\mathbf{x} \quad (26)$$

In our case, f and g are GPs defined by their mean and covariance functions. Detrending during data preprocessing ensures that the distributions have zero mean, $\mu_f = \mu_g = 0$. This simplifies the distance calculation to

$$D_B(f(\mathbf{x}), g(\mathbf{x})) = \frac{1}{2}\log\left(\frac{|\Sigma|}{\sqrt{|\Sigma_f||\Sigma_g|}}\right) \quad (27)$$

where

$$\Sigma = \frac{\Sigma_f + \Sigma_g}{2} \quad (28)$$

The Bhattacharyya distance for GPs is therefore only dependent on the choice of kernel and optimised hyperparameters. Estimation of each connection's GP hyperparameters is achieved by maximising the marginal likelihood of the data, and allows us to compute covariance matrices for each connection on a common input scale. Formation of a Bhattacharyya similarity structure follows straightforwardly from Equation (27), calculating the inverse distance between each GP pair.

IV.2 Bayesian Non Negative Matrix Factorisation

Inverse Bhattacharyya distances between GPs allows us to map the client dataset to a relational space, where every pair i, j of connections is given a similarity value s_{ij}. The resulting similarity matrix $\mathbf{S}$ is input as an adjacency structure to a Bayesian non-negative matrix factorisation (NMF) scheme [6], a method with a history of successful application to a diverse set of community detection challenges ranging from social network structure in ecological systems to maritime anomaly detection [7].

Table 6: *2-medoids clustering on the January 2013 dataset across 25 broker connections.*

2-medoids Cluster Centroid	Nodes Assigned
Centroid 3	2, 3, 4, 5, 6, 7, 11, 12, 15, 17, 19, 24
Centroid 9	1, 8, 9, 10, 13, 14, 16, 18, 20, 21, 22, 23, 25

In Bayesian NMF, communities are viewed as explanatory latent variables for the observed link weights in the adjacency structure. The latent clustering is produced by a factorisation $\mathbf{S} \simeq \mathbf{WH}$, $\mathbf{S} \in \mathbb{R}^{N\times N}, \mathbf{W} \in \mathbb{R}^{N\times K}, \mathbf{H} \in \mathbb{R}^{K\times N}$. The inner rank K and factor elements w_{ik}, h_{kj} are derived by Maximum a Posteriori inference, and provide a soft, probabilistic membership score for clients to each community. The framework is therefore capable of recognising communities that overlap.

We apply Bayesian NMF to the January 2013 EURUSD dataset comprised of 25 broker connections, and provide the resulting classification in Table 5. Bayesian NMF finds 2 main classes, with 4 nodes whose membership scores suggest overlap between the 2 communities.

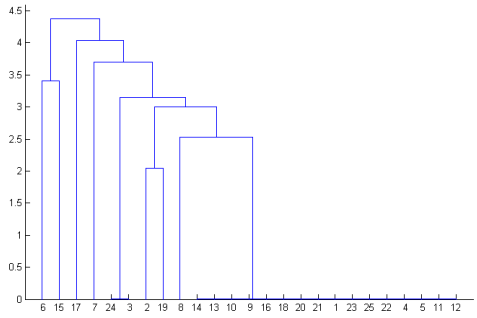

Figure 6: Dendrogram of the broker connections. Connections 14, 13, 10, 9, 16, 18, 20, 21, 1, 23, 25, 22, 4, 5, 11 and 12 present a very small distance from one another, identified by the low (<0.05) height at which the tree unites them. These brokers correspond exactly to Cluster 2 from Bayesian NMF, with the addition of the nodes found in the overlap. The remaining nodes can be thought of as a single other cluster, matching Cluster 1 from Bayesian NMF.

IV.3 Comparison to Benchmark Classifiers

For completeness, we compare the results to a hierarchical clustering dendrogram approach and k-medoids, with k set equal to the number of communities found by Bayesian NMF.

We define briefly the method of construction for dendrograms:

• The initial partition P_0 assigns each node to its own class.

• The final partition P_{n-1} (the conjoint partition) is one all-inclusive node class.

• P_{k+1} is defined from P_k by uniting a single pair of subsets in P_k. Union is pursued on the basis of closeness, where we minimise the maximum distance between any pair within the joined subsets (we minimise the subset 'diameter').

The resulting tree is provided in Figure 6.

In line with Bayesian NMF's discovery of 2 communities, we test our matrix of Bhattacharyya distances on a 2-medoids clustering algorithm, and report its results in Table 6.

In both cases, Bayesian NMF finds almost identical classes (node 8 is the sole exception) with two additional benefits. Firstly, it determines the appropriate number of classes k, obviating the need to hand-tune. Secondly, its soft partitioning allows the identification of nodes at the intersection of the classes. A graphical representation of the network's topology is provided in Figure 7, summarising the results of community detection.

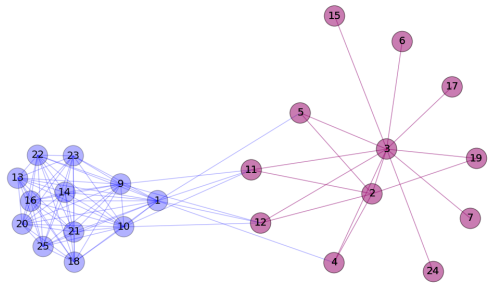

Figure 7: Colour-coded visualisation of the adjacency structure constructed from Bhattarcharya distances between each pair of broker connections. Note that Bayesian NMF placed nodes 4, 5, 11 and 12 in the overlap between the two clusters, and that the 2-medoid approach assigned nodes 3 and 9 as centroids for their respective clusters.

V. Integration to the Hamilton-Jacobi-Bellman Framework

Adverse selection represents opportunistic arbitrage of information asymmetry. We assume that such information advantages do not occur with any regularity in our polarity-insensitive GP regressions, and that adverse selection will therefore manifest as a highly entropic probability distribution over our feature space. For each connection i modelled as an ARD GP with covariance matrix $K_i \in \mathbb{R}^{D\times D}$, we compute its differential entropy as

$$H(i) = \frac{1}{2}\log\left((2\pi e)^D |K_i|\right) \tag{29}$$

Low entropy counterparties exhibit predictable trading activity, which eases the market maker's task of managing inventory risk. Conversely, highly entropic counterparties complicate the market maker's task and may, in our assumption, indicate an adverse selector. We therefore rank our list of counterparties by ascending entropy, and postulate that the inventory-optimal bid-mid and mid-offer solutions δ^b_{HJB} and δ^a_{HJB} from Equations (10) and (11) should be adjusted on a per-connection basis as a monotonically increasing function f of entropy, yielding broker-specific solutions

$$\delta^b(i) = \delta^b_{HJB} + f(H(i)) \tag{30}$$

and

$$\delta^a(i) = \delta^a_{HJB} + f(H(i)) \tag{31}$$

where the functional form of f is an open question, warranting further research.

In the event of an extremely large number of counterparties in the dataset, dimensionality can be first reduced by the community detection methods outlined earlier, and entropy adjustments calculated on representative centroids for each cluster.

VI. Conclusions

Adverse selection poses a client-specific risk hitherto insufficiently addressed by the literature on optimal market making. Our work provides a scalable basis for representing client behaviour and quantifying adverse selection via entropy. Designed to fit within the differential equations governing dynamic inventory risk management, our result bridges the state-of-the-art in stochastic control with novel techniques from the machine learning community. Far from being distinct research domains, the feedback mechanisms of control theory are a recurrent theme of reinforcement learning, where further work may provide an elegant synthesis to the market making challenges of inventory risk and adverse selection.

References

[1] Ho, T. and Stoll, H. (1981). Optimal dealer pricing under transactions and return uncertainty. *Journal of Financial Economics, 1981*.

[2] Avellaneda, M. and Stoikov, S. (2008). High-frequency trading in a limit order book. *Quantitative Finance, 2008*.

[3] Guéant, O., Lehalle, C. and Fernandez-Tapia, J. (2013). Dealing with the inventory risk: a solution to the market making problem. *Mathematics and Financial Economics, 2013*.

[4] Rasmussen, C. and Williams, C. (2006). Gaussian Processes for Machine Learning. *MIT Press*.

[5] Smith, M., Reece, S., Roberts, S., Psorakis, I. and Rezek, I. (2014). Maritime Abnormality Detection using Gaussian Processes. *Knowledge and Information Systems, March 2014, Volume 38*.

[6] Psorakis, I., Roberts, S., Ebden, M. et al. (2011). Overlapping community detection using Bayesian non-negative matrix factorisation. *Physical Review 83, 2011*.

[7] Psorakis, I., Rezek, I., Roberts, S. et al. (2012). Inferring social network structure in ecological systems from spatio-temporal data streams. *Journal of the Royal Society Interface 9, 2012*.